Available online at www.sciencedirect.com
ScienceDirect
Journal of Nuclear Materials 363–365 (2007) 534–538
journal of nuclear materials
www.elsevier.com/locate/jnucmat

Initial results of H-mode edge pedestal turbulence evolution with quadrature reflectometer measurements on DIII-D

G. Wang [a,*], W.A. Peebles [a], E.J. Doyle [a], T.L. Rhodes [a], L. Zeng [a], X. Nguyen [a], T.H. Osborne [b], P.B. Snyder [b], G.J. Kramer [c], R. Nazikian [c], R.J. Groebner [b], K.H. Burrell [b], A.W. Leonard [b], M.E. Fenstermacher [d], E.J. Strait [b]

[a] *University of California, Los Angeles, CA 90095, USA*
[b] *General Atomics, San Diego, CA 92186-5608, USA*
[c] *Princeton Plasma Physics Laboratory, Princeton, NJ 08543, USA*
[d] *Lawrence Livermore National Laboratory, Livermore, CA 94550, USA*

Abstract

High-resolution quadrature reflectometer measurements of density fluctuation levels have been obtained on DIII-D for H-mode edge pedestal studies. Initial results are presented from the L–H transition to the first ELM for two cases: (i) a low pedestal beta discharge, in which density turbulence in the pedestal has little change during the ELM-free phase, and (ii) a high pedestal beta discharge in which both density and magnetic turbulence are observed to increase before the first ELM. These high beta data are consistent with the existence of electromagnetic turbulence suggested by some transport models. During Type-I ELM cycles, when little magnetic turbulence can be observed, pedestal turbulence increases just after an ELM crash and then decreases before next ELM strikes, in contrast to a drop after ELM crash and then it re-grows when strong magnetic turbulence shows similar behavior. Clear ELM precursors are observed on $\leqslant$20% of Type-I ELMs observed to date.

PACS: 52.35.Ra; 52.40.Hf; 52.55.Fa; 52.70.−m

Keywords: Fluctuations and turbulence; Edge pedestal; ELM; Edge plasma; DIII-D

1. Introduction

High confinement mode (H-mode) tokamak operation is characterized by the spontaneous formation of a transport barrier at the edge, called the edge pedestal, which is often perturbed by repetitive edge localized modes or ELMs. Understanding the physics of the edge pedestal and ELMs is a key fusion science issue and a high priority for ITER for a couple of reasons. There is a strong dependence, both observed and predicted by transport models, of core confinement on the pressure at the top of the pedestal (or 'pedestal height') [1],

* Corresponding author. Address: C/o General Atomics, P.O. Box 85608, MS 13-353, San Diego, CA 92186, USA. Fax: +1 858 455 4156.
E-mail address: wangg@fusion.gat.com (G. Wang).

0022-3115/$ - see front matter © 2007 Elsevier B.V. All rights reserved.
doi:10.1016/j.jnucmat.2006.12.046

and ELMs transport bursts of particles and heat to the divertor plates which could pose a divertor erosion risk in a burning plasma device like ITER [2].

Significant progress has been made in this area of research in recent years [1–6]. However, many open questions still remain in understanding the edge pedestal and ELMs which impact their predictive modeling and control: e.g. what is the transport mechanism in the ELM-free H-mode pedestal, how does the pedestal evolve prior to and recover after an ELM? Recently, fixed-frequency quadrature reflectometers for measurement of low-k density fluctuations ($k_\perp < 6\ \mathrm{cm}^{-1}$) were successfully applied to DIII-D edge pedestal measurements [7]. These reflectometer systems have the advantage of high time resolution (100 μs in this study), high spatial resolution (sub-cm), high sensitivity and are nonperturbative. In addition, quantitative results are obtained using a full-wave 2-D interpretative code [8]. Results presented here are from an initial data set and address some of the pedestal and ELM issues mentioned above.

2. Quantitative density fluctuation measurements utilizing quadrature reflectometers on DIII-D

Two fixed-frequency reflectometers (42 and 65 GHz) utilizing quadrature phase detection have been installed on the DIII-D tokamak [7]. The launch and receive antennas of the systems are located external to the vacuum vessel on the low-field side, with the 65 GHz system horns positioned at a position 2.5 cm above the midplane, and the 42 GHz system horns 11 cm above the midplane. A 2-D full-wave code [8] is used to interpret the measured microwave electric field fluctuations, so as to deduce a density fluctuation level. This is done by simulating the reflectometer measurement using realistic geometry, plasma conditions, and antenna patterns. The code generates a prediction for the experimentally measured coherent reflection coefficient, defined as $G \equiv \frac{|\langle M \rangle|}{\sqrt{\langle |M|^2 \rangle}}$, where $\langle\,\rangle$ denotes an ensemble average, and M is the antenna quadrature electric field signal [9]. The assumed fluctuation level in the code is varied until the code value for G matches the experimental value. G is also used directly as an indicator of the density fluctuation level or of profile variations; a low density fluctuation level will scatter little microwave power, such that a strong specular reflection is obtained, and G is high. Therefore, G increases as the density fluctuation level decreases (though in general the relationship is nonlinear) [8,9]. Since density and electron temperature profiles are needed for the 2-D code modeling, quantitative density fluctuation levels are only obtained at the time of Thomson scattering measurements, i.e. typically every 12.5 ms. For higher time resolution, e.g. through ELMs, the experimentally measured G coefficient is plotted as an inverse measure of the fluctuation amplitude.

3. Turbulence observations during the ELM-free period leading to the first ELM

Two cases of turbulence behavior have been studied at low and high pedestal beta, as illustrated in Figs. 1 and 2. Shown in Fig. 1 are data from a discharge with low pedestal electron beta (ratio of pedestal electron to magnetic pressure), showing that the pressure pedestal height (Fig. 1(c)) and maximum gradient (Fig. 1(d)) increase continually during the ELM-free phase before the onset of the first ELM, while the density turbulence level displays no obvious change (Fig. 1(b)). The top of the pressure pedestal is located ~1.3 cm inside the separatrix, and the maximum gradient location is

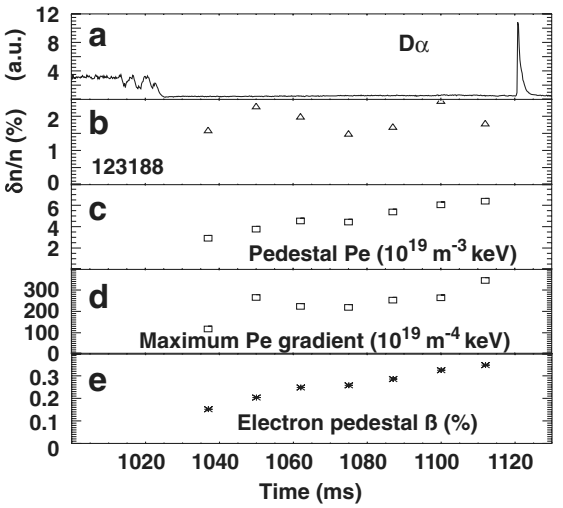

Fig. 1. Turbulence evolution prior to the first ELM for a low pedestal beta discharge 123188, with $I_p = 1.2$ MA, $B_T = 1.62$ T. (a) D_α time history, (b) density turbulence level in pedestal measured by 42 GHz reflectometer, (c) electron pressure pedestal height, and (d) maximum electron pressure gradient from Thomson scattering measurements, and (e) electron pedestal beta. (c) and (d) are calculated from TANH fits to the pressure profiles mapped to the outboard midplane using the EFIT equilibrium solver [10].

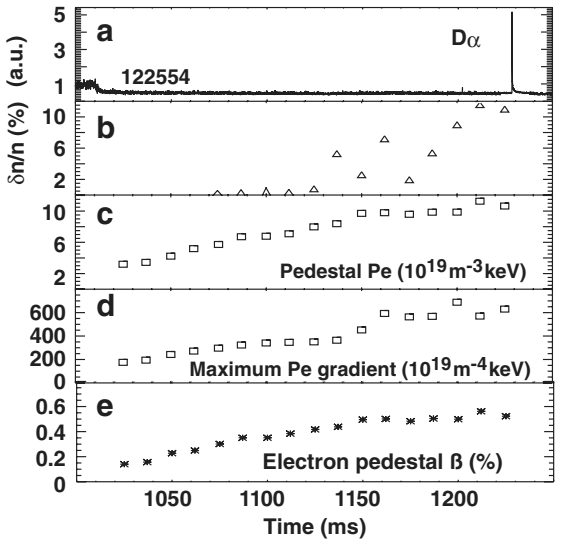

Fig. 2. Turbulence evolution prior to first ELM for a high pedestal beta discharge 122 554, with $I_p = 1.2$ MA, $B_T = 1.73$ T, with all plots corresponding to those in Fig. 1.

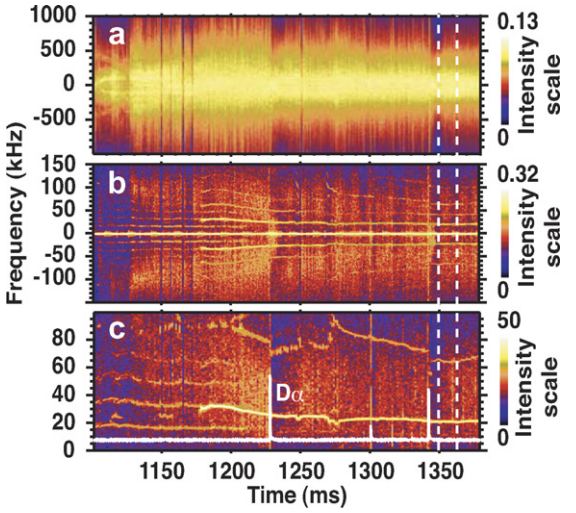

Fig. 3. Contour plot of frequency spectrum from (a) 42 GHz quadrature reflectometer system, (b) heterodyne FIR scattering measurement, and (c) magnetic loop $\dot{\boldsymbol{B}}$ signal, for first and subsequent ELMs in high pedestal beta discharge 122 554. The left vertical dashed line indicates the time just after an ELM when the turbulence drops, and the right one marks when the turbulence increases again.

~7 mm inside the separatrix on average. The detection location of the reflectometer is in the steep pedestal gradient region, ~3 mm inside the separatrix on average, with a standard deviation of ~2 mm. In this case, little and unchanged broadband fluctuations are observed on magnetic pickup coils.

In contrast, in a high pedestal beta discharge, Fig. 2, a large increase in turbulent density fluctuations (Fig. 2(b)) is observed in the pedestal, starting ~100 ms before the first ELM, and following an initial very low fluctuation level after L–H transition. In this case, the 42 GHz reflectometer channel was located ~1 cm inside the separatrix with a standard deviation of ~2.5 mm. The electron pressure pedestal height (Fig. 2(c)) appears to saturate at the same time that the pedestal turbulence starts to grow. A turbulence increase before the first ELM is simultaneously observed in reflectometry, far-infrared (FIR) scattering [11] low-k fluctuation data, and magnetic loop data from the outboard midplane, shown in Fig. 3(a)–(c), respectively. For all three signals the large amplitude, broadband turbulence decreases just after the first and several subsequent ELM crashes, and then re-grows until the next ELM strikes. The 42 GHz reflectometer measures a 4.1% density fluctuation level in the pedestal at 1350 ms when the turbulence in the FIR and magnetic signals drop after an ELM, as marked by the left vertical dashed line in Fig. 3, and 6% at 1362 ms after the turbulence increased again, as marked by the right vertical dashed line. In this case, the broadband magnetic fluctuations are more than one order of magnitude higher than that of Fig. 1. It can be noted in Fig. 3 that there are some coherent modes present which can be identified as tearing modes by comparing to magnetic loops measurement. These modes were excluded from the calculation of fluctuation levels from the reflectometer data.

The correlation of the magnetic and density fluctuation signals in time and frequency width through the initial ELMs in the high beta discharge suggest that the turbulence is electromagnetic in nature in this case. This observation points to the potential importance of electromagnetic effects on the transport in the edge pedestal and appears to be consistent with a prediction of electromagnetic turbulence by a 3-D gyrofluid simulation of pressure gradient driven microturbulence [12]. This simulation predicts strong electromagnetic turbulence effects as β (the ratio of plasma to magnetic pressure) is increased close to β_c, which is the local ideal ballooning limit. The proximity of the pedestal to β_c remains to be evaluated; detailed comparisons with theory of the above two cases and studies of a larger data set are planned as future work.

4. High time resolution measurements of turbulence behavior during Type-I ELMs

In this section, we consider the pedestal turbulence behavior during Type-I ELMs with high time resolution. In contrast to the observation shown in Fig. 3 where both pedestal turbulence and broadband magnetic fluctuations decrease just after ELM crashes, and then re-grows until the next ELM strikes, pedestal turbulence shows reversed behavior when little and unchanged broadband fluctuations (more than one order of magnitude lower) are observed on magnetic pickup coils later (start from ~1 s after the first ELM) in the high β discharge, as shown in Figs. 4 and 5.

Fig. 4(b) shows measurements of the edge density fluctuation level at two times in an ELM cycle; during the ELM crash, ~0.4 ms after the midplane D_α jumps, and ~12.1 ms before the ELM crash. Fig. 4(c) and (d) shows a comparison of Thomson scattering measured density and electron temperature radial profiles, respectively, at these two times, mapped to the outboard midplane, showing a clear collapse of the density pedestal. However, the location of the cutoff layer for the 42 GHz reflectometer, using O-mode polarization, is almost unchanged. The turbulence level in the pedestal changed from a low level of 0.3% prior to the ELM to 1.6% at the ELM crash, as plotted in Fig. 4(b). This observation is consistent with the proposition that at an ELM crash, one of the mechanisms for the rapid loss of particles and heat from the edge region is a

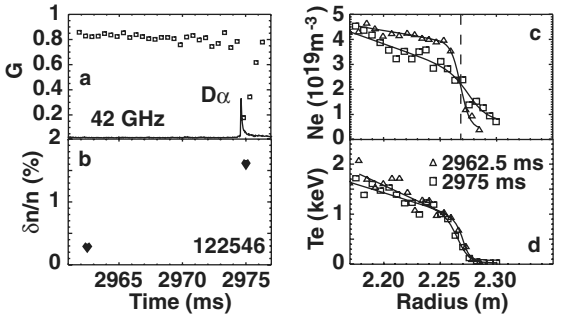

Fig. 4. Fluctuation levels before and during an ELM for discharge 122546, a similar shot as 122554. (a) Coherent reflection coefficient G versus time for 42 GHz reflectometer and D_α time history, (b) density turbulence level measured by the reflectometer at two time slices, and (c) radial density and (d) temperature profiles mapped to the outboard midplane for the time slices measured by Thomson scattering. The vertical dashed line in (c) marks the cutoff location of the 42 GHz reflectometer using O-mode polarization.

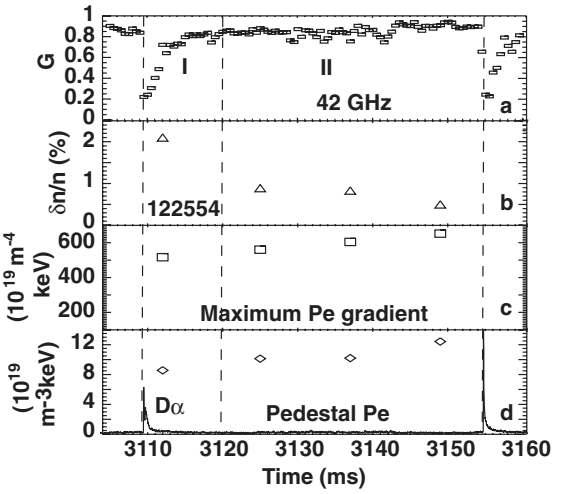

Fig. 5. Fluctuation data covering a full ELM cycle in discharge 122554. (a) Coherent reflection coefficient G versus time for reflectometer data, (b) density turbulence level, (c) maximum electron pressure gradient, and (d) electron pressure pedestal height, as well as D_α time history.

temporary return to L-mode-like edge transport due to a collapse of the edge transport barrier [13].

Plotted in Fig. 5 are measurements taken during a full ELM cycle. The measured coherent reflection coefficient G, shown in Fig. 6(a) indicates that the inter-ELM period consists of two distinct phases: Phase I with fast density profile recovery and/or fluctuation change, generally persisting for <10 ms, and Phase II with slow density gradient evolution and/or fluctuation change. This observation is consistent with previous high-resolution density profile measurements on DIII-D (see Fig. 2 in [14]) and ASDEX Upgrade [15], showing a fast density profile recovery just after a Type-I ELM crash, followed by

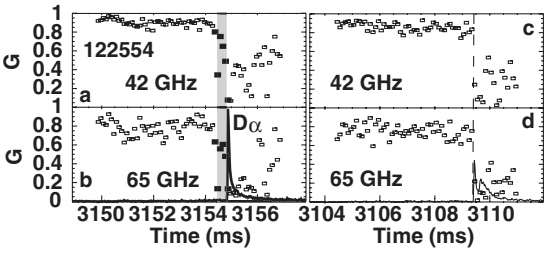

Fig. 6. Coherent reflection coefficient G versus time for (a), (c) 42 GHz and (b), (d) 65 GHz reflectometers, with D_α time history. The left hand panels [(a) and (b)] are for an ELM with a clear precursor (marked by shaded band), while the right hand panels [(c) and (d)] are for an ELM without a precursor, both from discharge 122554.

a slow increase leading to the next ELM. Maximum gradient and pedestal height for the electron pressure are plotted in Fig. 6(c) and (d) respectively, showing that these quantities increase from Phase I to II. Correspondingly, density turbulence levels from the 42 GHz reflectometer system are plotted in Fig. 5(b), using G averaged over 4 ms. The detection locations of the reflectometer vary within 4 mm and are $\sim$7 mm inside the separatrix on average. The fluctuation level exhibits a drop toward the second ELM. The reversed pedestal turbulence behavior (compared to Fig. 3) shown here and in Fig. 4 suggests important role of magnetic turbulence in ELM dynamics.

We now address the potential role of turbulence as an ELM trigger mechanism, where two cases are observed, as shown in Fig. 6, with and without clear ELM precursors in the reflectometer signal. In the case of an ELM with a precursor (left panels in Fig. 6), the coherent reflection coefficient G (inversely proportional to fluctuation level) of the two reflectometer channels start to decrease $\sim$0.4 ms before the abrupt jump in midplane D_α. In contrast, in the case of the right panels, the G values only drop sharply coincident with the D_α jump, with no precursor. Both examples shown are from a single discharge. It is not yet clear why precursors are observed on some ELMs but not others; in the limited data set obtained so far, precursors are observed on $\leqslant$20% of Type-I ELMs. Future work in this area will focus on a detailed evaluation of whether the 3-D character of Type-I ELM onset [13] can explain these observations, but a preliminary evaluation is that the ELM precursors, when observed, persist for too long to be consistent with this potential explanation.

5. Summary and conclusions

In summary, this paper reports initial results from new quantitative pedestal turbulence measurements utilizing quadrature reflectometers on DIII-D. After the L–H transition and before the first ELM, turbulence in the pedestal does not change in a low pedestal beta discharge, while a significant increases in turbulence with an electromagnetic character was observed before the first ELM in a high pedestal beta discharge. This result suggests that electromagnetic effects may be playing a role in pedestal transport under some conditions. During Type-I ELM cycles, when little magnetic turbulence can be observed, pedestal turbulence increases just after an ELM crash and then decreases before next ELM strikes, in contrast to a drop after ELM crash and then it re-grows when strong magnetic turbulence shows similar behavior. Precursor activity is observed before a minority ($<$20%) of Type-I ELMs; why such precursor activity is observed before some but not all ELMs requires further study.

Acknowledgement

Work supported by US DOE under DE-FG03-01ER54615, DE-FC02-04ER54698, DE-AC02-76CH03073, and W-7405-ENG-48.

References

[1] P.B. Snyder et al., Nucl. Fus. 44 (2004) 320.
[2] G.T.A. Huysmans, Plasma Phys. Control. Fus. 47 (2005) B165.
[3] J.W. Connor, Plasma Phys. Control. Fus. 40 (1998) 191.
[4] W. Suttrop, Plasma Phys. Control. Fus. 42 (2000) A1.
[5] A.E. Hubbard, Plasma Phys. Control. Fus. 42 (2000) A15.
[6] M.E. Fenstermacher et al., Nucl. Fus. 45 (2005) 1493.
[7] G. Wang et al., Nucl. Fus. 46 (2006) S708.
[8] E.J. Valeo, G.J. Kramer, R. Nazikian, Plasma Phys. Control. Fus. 44 (2002) L1.
[9] G.J. Kramer, R. Nazikian, E.J. Valeo, Rev. Sci. Instrum. 74 (2003) 1421.
[10] L.L. Lao et al., Nucl. Fus. 30 (1990) 1035.
[11] T.L. Rhodes, et al., in: Proceedings of the 20th IAEA Fusion Energy Conference, Vilamoura, 2004.
[12] P.B. Snyder, Hammett, Phys. Plasma 8 (2001) 745.
[13] P.B. Snyder et al., Phys. Plasma 12 (2005) 056115.
[14] L. Zeng et al., J. Nucl. Mater. 336–339 (2005) 742.
[15] I. Nunes et al., Nucl. Fus. 44 (2004) 883.